APPENDICE A

PAPER

Scripta Materialia 133 (2017) 96–100

Contents lists available at ScienceDirect

Scripta Materialia

journal homepage: www.elsevier.com/locate/scriptamat

Regular Article

Effect of the crystal structure on the electronic structure and electrical properties of thermoelectric $GeSb_6Te_{10}$ prepared by hot pressing

Wanatchaporn Namhongsa [a,b,c], Tatsuro Omoto [a], Yosuke Fujii [d], Tosawat Seetawan [b,c], Atsuko Kosuga [a,*]

[a] Department of Physical Science, Graduate School of Science, Osaka Prefecture University, Sakai 599-8531, Japan
[b] Program of Physics, Faculty of Science and Technology, Sakon Nakhon Rajabhat University, Sakon Nakhon 47000, Thailand
[c] Thermoelectric Research Laboratory, Center of Excellence on Alternative Energy, Research and Development Institution, Sakon Nakhon Rajabhat University, Sakon Nakhon 47000, Thailand
[d] Department of Mathematical Science, Graduate School of Engineering, Osaka Prefecture University, Sakai 599-8531, Japan

ARTICLE INFO

Article history:
Received 14 December 2016
Accepted 6 February 2017
Available online xxxx

Keywords:
Homologous compound
X-ray diffraction
Electronic structure
Electrical properties

ABSTRACT

$GeSb_6Te_{10}$ is a potential thermoelectric material for the middle-temperature range, but its crystal structure is significantly affected by the preparation process, possibly leading to differences in the electrical properties depending on the preparation process. In the present study, the crystal structure and electrical properties of hot-pressed $GeSb_6Te_{10}$ were experimentally investigated and compared with those of melt-prepared and spark plasma sintering (SPS)-consolidated samples. We also discuss how changes in the crystal structure induced after hot pressing would affect the electronic band structure of the sample using the results of first-principles calculations within the framework of density functional theory.

Ge–Sb–Te materials have recently attracted much attention not only as high-speed phase change materials, but also as potential thermoelectric (TE) materials [1–3]. Among the Ge–Sb–Te materials, $(GeTe)_n(Sb_2Te_3)_m$ homologous (HG) compounds (where n and m are integers) with long-period crystal structures are regarded as good performance TE materials [3–5]. This is because such materials are expected to possess low lattice thermal conductivity, which is a desirable property for TE materials. The HG compounds have heavy constituent elements in large unit-cells with relatively weak van der Waals (vdW) forces between slabs, both of which lead to strong phonon scattering. In our previous study [6], we focused on $GeSb_6Te_{10}$ existing as a Sb_2Te_3-rich HG compound in the $GeTe–Sb_2Te_3$ pseudobinary system [7]. $GeSb_6Te_{10}$ has a rhombohedral structure belonging to the space group $R\text{-}3m$ with 51 atoms in the unit cell. In the unit cell, it form a covalently bonded quintuple Sb_2Te_3 layer (—Te–Sb–Te–Sb–Te–, denoted S5) and septuple $GeSb_2Te_4$ layer (—Te–Sb–Te–Ge–Te–Sb–Te–, denoted S7) in the sequence (S5–S7–S5)(S5–S7–S5)(S5–S7–S5), where the bonding between S5 and S7, and S5 and S5 is by weak vdW interactions. Detailed crystal structure analysis revealed that Te atoms occupy their own specific layers, whereas Ge and Sb atoms are randomly located in their layers [8]. First, we attempted to enhance the TE properties by elemental doping [6]. As a result, the TE properties of melt-prepared $GeSb_6Te_{10}$ doubled by In doping into the Sb site by lowering the lattice thermal conductivity and improving the electrical properties. We then prepared sintered $GeSb_6Te_{10}$ by spark plasma sintering (SPS) for practical applications, and clarified that the compositional deviation and evolution of the Sb_2Te_3 structure were induced by the SPS process [9]. We presumed that this arose from the unique heating method of SPS. In the SPS method, the powders are placed in a die and heated using a pulsed electric current while applying a uniaxial pressure. The conducting powders are heated not only by thermal conduction from the die, but also by the Joule effect. This can lead to local overheating and cause changes in the constituent phases and crystal structure of $GeSb_6Te_{10}$ during the SPS process, which has been observed in other TE materials [10,11].

In the present study, hot pressing was used to consolidate a powder sample of $GeSb_6Te_{10}$. Differing from the SPS process, hot pressing makes use of thermal conduction from the die while applying heat to the powder, so we expected that a compositionally and structurally homogeneous sample would be obtained. Surprisingly, we obtained a mixture of $GeSb_6Te_{10}$ and Sb_2Te_3 structures in the hot-pressed $GeSb_6Te_{10}$ sample. This result indicates that $GeSb_6Te_{10}$ is rather unstable against heat treatment with pressure compared with its end members Sb_2Te_3 and GeTe, which do not show any structural modification and/or evolution of other structures with SPS and hot pressing [12,13]. We also discuss how changes in the crystal structure induced after hot press would affect the electronic structure of the sample using the results of first-principles calculations within the framework of density functional theory (DFT), and compare the results with the experimentally obtained electrical properties.

The hot-pressed sample of polycrystalline $GeSb_6Te_{10}$ (GST-hotpress) was purchased from China Rare Metal Material Co., Ltd. The sample was in the form of a disk with dimensions of 38.15 mm in diameter and

* Corresponding author.
E-mail address: a-kosuga@p.s.osakafu-u.ac.jp (A. Kosuga).

http://dx.doi.org/10.1016/j.scriptamat.2017.02.013
1359-6462/

5.02 mm in thickness. The crystal structure of the sample was determined by powder X-ray diffraction (XRD) at room temperature with Cu-Kα radiation, and analyzed by Rietveld analysis using Jana 2000 software [14]. The elemental composition of the sample was determined by energy-dispersive X-ray spectroscopy at room temperature at an accelerating voltage of 15 keV.

The theoretical calculations were performed using the projector augmented-wave method [15,16] within the framework of DFT [17,18], as implemented in the Vienna ab initio simulation packages (VASP). The Perdew–Burke–Ernzerhof exchange correlation functional was used with the generalized gradient approximation (GGA–PBE) [19]. For the total energy calculation and structural optimization, the energy cutoff was set to 500 eV and the Brillouin zone was sampled with $5 \times 5 \times 1$ Monkhorst–Pack k-point meshes. Both the lattice parameters and atom coordinates of the initial structure given by the Rietveld analysis were relaxed. The atomic positions were relaxed until the magnitude of the force acting on each atom became less than 0.02 eV $Å^{-1}$. The energy convergence criterion was chosen to be 10^{-7} eV. Based on the relaxed crystal structures, the density of states (DOS) curves and electronic band structure were calculated. The $5 \times 5 \times 5$ k-point meshes were automatically generated with their origin at the Γ point, and the tetrahedron method with Blöchl corrections [20] was used.

The electrical conductivity σ and Seebeck coefficient S values of GST were measured by the standard four-probe method using a commercially available apparatus (ZEM-3; ULVAC Technologies) at 300–673 K in helium atmosphere. The power factor $S^2\sigma$ was evaluated at 300–673 K in helium atmosphere using the measured σ and S values.

Fig. 1(a) shows the XRD pattern of GST-hotpress, together with those of GST-melt [6] and GST-anneal [9]. GST-melt and GST-anneal are polycrystalline samples of $GeSb_6Te_{10}$ prepared by melting and by SPS and subsequent annealing, respectively. The overall XRD pattern of GST-hotpress is quite similar to those of GST-melt and GST-anneal. However, there is an obvious difference in the range $2\theta = 16–20°$ (Fig. 1(b)). In this range, GST-melt has a single peak corresponding to 0021_{HG} (HG represents a Bragg peak of the $GeSb_6Te_{10}$-type homologous structure), whereas GST-anneal has a new satellite peak corresponding to 006_{TD} (TD represents a Bragg peak of the Sb_2Te_3-type tetradymite structure) at the lower-angle side of 0011_{HG}. For GST-hotpress, the intensity of the 006_{TD} peak is higher than that of the 0021_{HG} peak. Other peaks in different angle ranges show the same tendency (a typical example is shown in Fig. 1(c)). Based on this finding, we performed Rietveld analysis assuming that GST-hotpress contains the $GeSb_6Te_{10}$-type HG structure and the Sb_2Te_3-type TD structure, and the data fitted well to a previously reported model [8] (see Fig. S1 in Supplemental Material). The obtained phase fraction ratio of the $GeSb_6Te_{10}$ structure to the Sb_2Te_3 structure is ca. 40 to 60 wt.%. These results indicate that GST-hotpress contains not only the $GeSb_6Te_{10}$ structure but also the Sb_2Te_3 structure.

To investigate how evolution of the Sb_2Te_3 structure in the sample affected its electrical properties, we compared the density of states (DOS) of $GeSb_6Te_{10}$ and its end members GeTe and Sb_2Te_3. Fig. 2 shows the orbital projected DOS of the GeTe, $GeSb_6Te_{10}$, and Sb_2Te_3 structures. For $GeSb_6Te_{10}$ and Sb_2Te_3, Te p and Sb s orbitals significantly contribute to the valence-band edge, whereas Sb p and Te p orbitals contribute to the conduction-band edge of the band gap. For GeTe, Te p and Ge s orbitals contribute to the valence-band edge, whereas Ge p and Te p orbitals contribute to the conduction-band edge of the band gap. The DOS curve of $GeSb_6Te_{10}$ is relatively similar to that of Sb_2Te_3. We consider that this is a reasonable result taking into account the structural similarity of $GeSb_6Te_{10}$ and Sb_2Te_3. $GeSb_6Te_{10}$ has six units of the Sb_2Te_3 layer and three units of the $GeSb_2Te_4$ layer in its structure. Because of the similarity with the $GeBi_2Te_4$ structure, as reported by Kooi et al. [21], the $GeSb_2Te_4$ structure can be considered to be the multiblock structure, in which GeTe structure inserted in the middle of Sb_2Te_3 quintuple layers, that is, the structure of $GeSb_6Te_{10}$ is mainly composed of Sb_2Te_3. Therefore, the electronic structure of $GeSb_6Te_{10}$

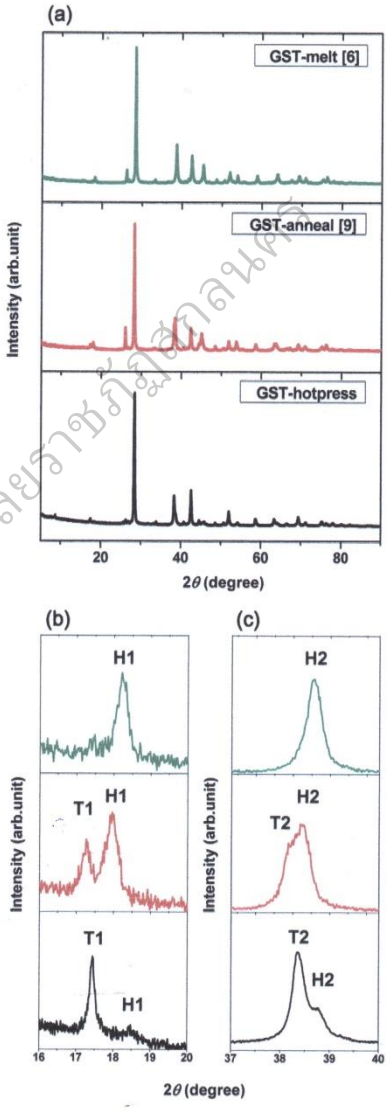

Fig. 1. (a) XRD patterns of GST-hotpress, GST-melt [6], and GST-anneal [9]. (b) Enlarged images in the range $2\theta = 16–20°$. The left peak corresponds to the Bragg peak of the 0 0 6 tetradymite structure (denoted T1) and the right peak is that of the 0 0 21 homologous structure (denoted H1). (c) Enlarged images of the range $2\theta = 37–40°$. The left peak corresponds to the Bragg peak of the 1 0 10 tetradymite structure (denoted T2) and the right peak is that of the 1 0 34 homologous structure (denoted H2).

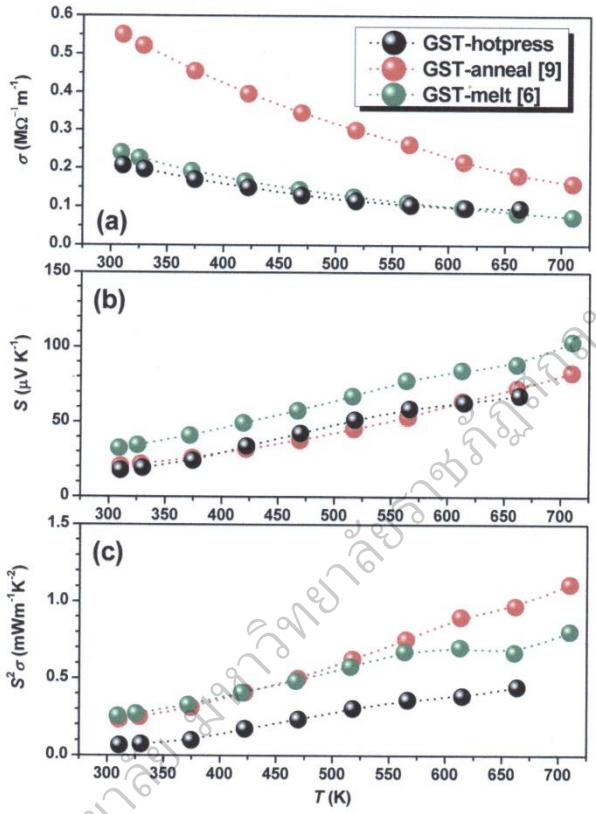

Fig. 2. (a) Orbital projected DOS of GeTe, $GeSb_6Te_{10}$, and Sb_2Te_3.

would be more similar to that of Sb_2Te_3 than that of GeTe. The electronic band structure of $GeSb_6Te_{10}$ also shows a direct band gap at the Γ point analogous to Sb_2Te_3 (Fig. S2 in Supplemental Material). Moreover, the obtained band-gap energy (E_g) decreases with increasing Sb content: GeTe (0.98 eV) > $GeSb_6Te_{10}$ (0.52 eV) > Sb_2Te_3 (0.27 eV). A systematic study of the electronic band structures of GeTe–Sb_2Te_3 pseudobinary compounds, such as GeTe, $Ge_2Sb_2Te_5$, $Ge_1Sb_2Te_4$, $Ge_1Sb_4Te_7$, and Sb_2Te_3, using ab initio calculations has been reported [22]. It was found that the direct/indirect band gap and band-gap width depend on the composition. With increasing Sb content, the compounds change from indirect band gap to direct band gap compounds. GeTe, $Ge_2Sb_2Te_5$, and $Ge_1Sb_2Te_4$ have an indirect band gap, whereas $Ge_1Sb_4Te_7$ and Sb_2Te_3 have a direct band gap. Moreover, the band-gap energy decreases as the Sb content increases. Considering these results, our results are reasonable. We conclude that the band structure of $GeSb_6Te_{10}$ has an indirect band gap, similar to Sb_2Te_3, but the band gap width is wider than that of Sb_2Te_3. Moreover, it is noteworthy that the slope of the DOS in the valence-band edge near the Fermi level of $GeSb_6Te_{10}$ is steeper than that of Sb_2Te_3, as shown in Fig. S3 in Supplemental Material. Because S is proportional to the slope of the DOS around the Fermi energy, we predict that the $GeSb_6Te_{10}$ structure has a higher S value than the Sb_2Te_3 structure. Although the ρ value of a material is affected by both the band structure and macroscopic factors (i.e., the bulk density and morphology), the S value is considered to be mainly affected by the electronic structure. Here, we will discuss how evolution of the Sb_2Te_3 structure in GST-hotpress would affect S under the hypothesis that GST-hotpress should exhibit more Sb_2Te_3 characteristics than $GeSb_6Te_{10}$ characteristics because the former is a mixture of Sb_2Te_3 and $GeSb_6Te_{10}$ structures and the latter is only $GeSb_6Te_{10}$ structure. A narrow band gap in a material generally leads to pronounced bipolar conduction at elevated temperatures. Our calculated results show that the Sb_2Te_3 structure has the maximum S at a lower temperature than the maximum S of the $GeSb_6Te_{10}$ structure, because holes and electrons contribute to conduction. Therefore, we predict that GST-hotpress would show bipolar conduction at lower temperature and have a lower S value than the $GeSb_6Te_{10}$ structure

(i.e., GST-melt). In addition, the curve of the DOS around the Fermi level for Sb_2Te_3 is shallower than that for $GeSb_6Te_{10}$, which leads to a lower S value. We suggest that this results in the lower S of GST-hotpress than GST-melt.

Fig. 3(a)–(c) show the temperature dependences of the electrical properties (i.e., σ, S, and $S^2\sigma$) of GST-hotpress along with those of GST-melt and GST-anneal. For GST-hotpress, σ decreases with increasing temperature from 0.208 $M\Omega^{-1}$ m^{-1} at 310 K to 0.0965 $M\Omega^{-1}$ m^{-1} at 664 K, and S increases with increasing temperature from 17.9 $\mu V\ K^{-1}$ at 310 K to 67.8 $\mu V\ K^{-1}$ at 664 K. Because all of the samples do not appear to show bipolar conduction within the measured temperature range, we are not able to confirm our prediction. The temperature dependences observed here show the characteristic behavior of degenerate semiconductors. GST-hotpress shows the same tendency as GST-melt and GST-anneal, but the values are slightly different. In particular, the lower S values of GST-hotpress and GST-anneal than those of GST-melt can be attributed to the shallower DOS curve of Sb_2Te_3 than $GeSb_6Te_{10}$, because the former two samples contain both $GeSb_6Te_{10}$ and Sb_2Te_3 structures, whereas the latter sample only contains the $GeSb_6Te_{10}$ structure. As a result, the maximum value of $S^2\sigma$ for GST-hotpress is 0.44 $mWm^{-1}\ K^{-2}$ at 663 K, which is smaller than those for GST-melt (0.97 $mWm^{-1}\ K^{-2}$ at 662 K) and GST-anneal (0.67 $mWm^{-1}\ K^{-2}$ at 661 K).

GST-hotpress has elemental compositional deviation, which is possibly correlated with the existence of two crystal structures ($GeSb_6Te_{10}$ and Sb_2Te_3). Compositional analysis of GST-hotpress was performed at 50 randomly selected points within a surface area of ca. 52 × 76 μm^2. The obtained results are summarized in Table S1 in Supplemental Material. The average composition of each element in GST-hotpress is closer to the nominal composition than the compositions of GST-melt and GST-anneal. This can be attributed to the different preparation conditions of the ingot samples of GST-melt, GST-anneal, and GST-SPS. The ingot samples of GST-anneal and GST-melt samples were prepared by ourselves using the same conditions (e.g., keeping temperature and time) [6,9], whereas the GST-hotpress sample was obtained from a company and the preparation conditions would not have been the same as those of the other two samples. For this reason, we will not further discuss the differences in the average values. Instead, we will focus on the standard deviations. From Table S1 in Supplemental Material, all of the elements in GST-hotpress and GST-anneal have larger standard deviation than those of GST-melt. To analyze this data in more detail, for the raw data, the cation (Ge plus Sb) content is plotted against the anion (Te) content in Fig. 4(a), and the cation content is plotted against the Ge content in Fig. 4(b), along with the average values of the present study and the nominal compositions of $GeSb_6Te_{10}$ and Sb_2Te_3. In general, points with higher cation content have higher Ge content (right-hand side in the figures), whereas points with lower cation content have lower Ge content (left-hand side in the figures). Assuming that each point corresponds to a mixture of Sb_2Te_3 and $GeSb_6Te_{10}$ phases with a different ratio, we can say that points located on the right-hand side of the figures have a high content of the Sb_2Te_3 phase, whereas points on the left-hand side of the figures have a higher content of the $GeSb_6Te_{10}$ phase. From Fig. 4(a), the cation content varies from 39.59 to 42.44 at.% for the 50 points. If each point is composed of a mixture of the stoichiometric compositions of Sb_2Te_3 and $GeSb_6Te_{10}$, the cation

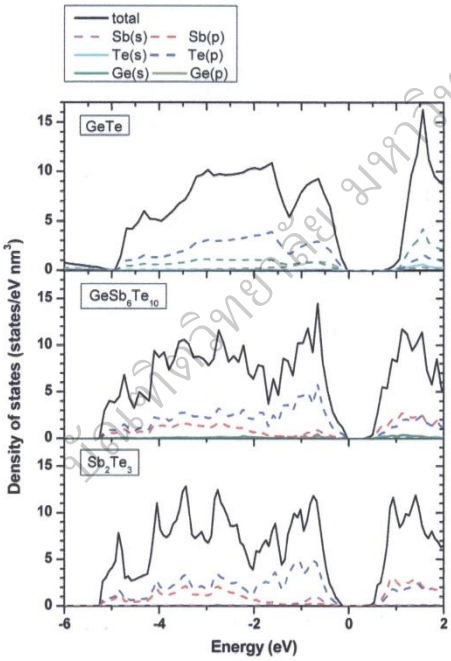

Fig. 3. Temperature dependences of the (a) electrical conductivity σ, (b) Seebeck coefficient S, and (c) power factor $S^2\sigma$ of GST-hotpress along with those of GST-melt [6] and GST-anneal [9]. The uncertainties of σ and S are within 5% and 7%, respectively.

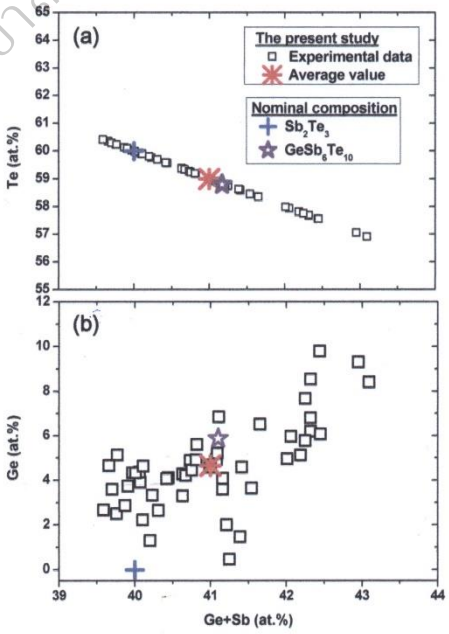

Fig. 4. (a) Ge + Sb content plotted against Te content. (b) Ge + Sb content plotted against Ge content. The calculated coefficient of correlation of (b) is 0.668, which means that there is a relatively strong correlation between the two factors.

contents for all the points should vary within the range 40–41.1 at.%, because the cation contents of Sb_2Te_3 and $GeSb_6Te_{10}$ are 40 and 41.4 at.%, respectively. This indicates that there is an off-stoichiometric composition of Sb_2Te_3 and $GeSb_6Te_{10}$ in the samples. Because it is known that a point defect V_{Ge} and an antisite defect Sb_{Te} readily form in GeTe and Sb_2Te_3 [23,24], resulting in an off-stoichiometric composition, a similar type of defect may form in GST-hotpress. Because the off-stoichiometric composition would also affect the band structure of the sample, further analysis of possible defects in the $GeSb_6Te_{10}$ structure is needed to discuss the results in detail.

In summary, we have investigated the effect of the crystal structure on the electronic structure and electrical properties of $GeSb_6Te_{10}$ prepared by hot pressing. GST-hotpress is composed of a mixture of $GeSb_6Te_{10}$ and Sb_2Te_3 structures with a ratio of ca. 40 wt.% to 60 wt.%, while the melt-prepared sample is composed of only $GeSb_6Te_{10}$ structure. Based on band structure calculations, we predict that GST-hotpress would show bipolar conduction at lower temperature and have a lower S value than GST-melt. The lower S value for GST-hotpress than GST-melt is because of the shallower curve of the DOS around the Fermi level for the Sb_2Te_3 structure than for the $GeSb_6Te_{10}$ structure. For GST-hotpress, the electrical conductivity decreases and the Seebeck coefficient increases with increasing temperature, which are the same tendencies as GST-melt, except that there are slight differences in the values of both properties. In particular, the lower Seebeck coefficient of GST-hotpress than GST-melt can be attributed to the shallower DOS curve of Sb_2Te_3 than $GeSb_6Te_{10}$, because the former sample contains both $GeSb_6Te_{10}$ and Sb_2Te_3 structures, whereas the latter sample only contains $GeSb_6Te_{10}$ structure. As a result, the maximum value of $S^2\sigma$ for GST-hotpress is 0.44 $mWm^{-1}K^{-2}$ at 663 K, which is smaller than the maximum $S^2\sigma$ values for GST-melt (0.97 $mWm^{-1}K^{-2}$ at 662 K) and GST-anneal (0.67 $mWm^{-1}K^{-2}$ at 661 K).

This work was partly supported by the Nippon Sheet Glass Foundation for Materials Science and Engineering, and the Program to Support Research Activities of Female Researchers in Osaka Prefecture University. W.N. was supported by research funding for master degree students from The Research and Researchers for Industry Program, RRI, Thailand. We thank Prof. Dr. Y. Kubota for his advice with the Rietveld analysis and Dr. P. Eaksuwanchai for her helpful technical support.

Appendix A. Supplementary data

Supplementary data to this article can be found online at http://dx.doi.org/10.1016/j.scriptamat.2017.02.013.

References

[1] M. Wuttig, N. Yamada, Nat. Mater. 6 (2007) 824–832.
[2] T. Matsunaga, N. Yamada, K. Kifune, Y. Kobuta, J. Cryst. Soc. Jpn. 51 (2009) 292–299.
[3] L.E. Shelimova, O.G. Karpinskii, P.P. Konstantinov, M.A. Kretova, E.S. Avilov, V.S. Zemskov, Inorg. Mater. 37 (2001) 342–348.
[4] P.P. Konstantinov, L.E. Shelimova, E.S. Avilov, M.A. Kretova, V.S. Zemskov, Inorg. Mater. 37 (2001) 662–668.
[5] E.-R. Sittner, K.S. Siegert, P. Jost, C. Schlockermann, F.R.L. Lange, M. Wuttig, Phys. Status Solidi A. 210 (2013) 147–152.
[6] A. Kosuga, K. Nakai, M. Matsuzawa, Y. Fujii, R. Funahashi, T. Tachizawa, Y. Kubota, K. Kifune, APL Mater. 2 (2014) 086102.
[7] N.K. Abrikosov, G.T.D. Dobryakova, Izv. Akad. Auk. SSSR Neorg. Mater. 1 (1965) 204–209.
[8] T. Matsunaga, R. Kojima, N. Yamada, T. Fujita, K. Kifune, Y. Kubota, M. Takata, Acta Crystallogr. Sect. B 66 (2010) 407–411.
[9] A. Kosuga, K. Nakai, M. Matsuzawa, Y. Fujii, R. Funahashi, T. Tachizawa, Y. Kubota, K. Kifune, J. Alloys Compd. 618 (2014) 463–468.
[10] J. Fan, H. Liu, X. Shi, S. Bai, X. Shi, L. Chen, Acta Mater. 61 (2013) 4297–4304.
[11] K. Kurosaki, T. Maekawa, H. Muta, S. Yamanaka, J. Alloys Compd. 397 (2005) 296–299.
[12] Y. Ma, Q. Hao, B. Poudel, Y. Lan, B. Yu, D. Wang, G. Chen, Z. Ren, Nano Lett. 8 (2008) 2580–2584.
[13] L. Yang, J.Q. Li, R. Chen, Y. Lin, F.S. Liu, W.Q. Ao, J. Electron. Mater. 45 (2016) 5533–5539.
[14] V. Petricek, M. Dusek, JANA2000, Academy of Sciences of the Czech Republic, Prague, Institute of Physics, 2000.
[15] P.E. Blöchl, Phys. Rev. B 50 (1994) 17953.
[16] G. Kresse, J. Joubert, Phys. Rev. B 59 (1999) 1758.
[17] G. Kresse, J. Hafner, Ab initio molecular dynamics for liquid metals, Phys. Rev. B 47 (1993) 558 (R).
[18] G. Kresse, J. Hafner, Phys. Rev. B 49 (1994) 14251.
[19] J.P. Perdew, K. Burke, M. Ernzerhof, Phys. Rev. Lett. 77 (1996) 3865.
[20] P.E. Blöchl, O. Jepsen, O.K. Andersen, Phys. Rev. B: Condens. Matter Mater. Phys. 49 (1994) 16223–16233.
[21] B.J. Kooi, J.T.M. De Hosson, J. Appl. Phys. 92 (2002) 3584.
[22] J.-W. Park, S.H. Eom, H. Lee, Phys. Rev. B 80 (2009) 115209.
[23] A.H. Edwards, A.C. Pineda, P.A. Schultz, M.G. Martin, A.P. Thompson, H.P. Hjalmarson, J. Phys. Condens. Matter 17 (2005) L329–L335.
[24] J. Horak, L. Koudelka, J. Klikorka, React. Solids 5 (1988) 351–359.